Research Square

Preprints are preliminary reports that have not undergone peer review.
They should not be considered conclusive, used to inform clinical practice,
or referenced by the media as validated information.

Comparative genomic and evolutionary analyses of receptor-like kinase genes across grasses and their expression dynamics in oat during leaf spot infection

Yanan Cao
Gansu Agricultural University
Jikuan Chai
Gansu Agricultural University
Kuiju Niu
Gansu Agricultural University
Liang Zeng
Gansu Agricultural University
Wenping Wang
Gansu Agricultural University
Panpan Huang
Gansu Agricultural University
Yanming Ma
Gansu Agricultural University
Guiqin Zhao
zhaogq@gsau.edu.cn
Gansu Agricultural University

Research Article

Keywords: Avena sativa, receptor-like kinase, gene family evolution, gene duplication, Drechslera avenae, weighted gene co-expression network analysis

Posted Date: November 21st, 2026

DOI: https://doi.org/10.21203/rs.3.rs-11675507/v1

License: This work is licensed under a Creative Commons Attribution 4.0 International License.
Read Full License

Additional Declarations: No competing interests reported.

Comparative genomic and evolutionary analyses of receptor-like kinase genes across grasses and their expression dynamics in oat during leaf spot infection

Yanan Cao[1], Jikuan Chai[1], Kuiju Niu[1], Liang Zeng[1], Wenping Wang[1], Panpan Huang[1], Yanming Ma[1], Guiqin Zhao[1*]

[1] Pratacultural College, Gansu Agricultural University, Lanzhou 730070, Gansu Province, People's Republic of China.

***Corresponding author:** Guiqin Zhao

Address: No. 1, Anning District, Lanzhou city, Gansu Province, China.

E-mail address: zhaogq@gsau.edu.cn

Abstract

Background: Oat (*Avena sativa* L.) is an important cereal and forage crop, but its production can be adversely affected by leaf spot disease. Receptor-like kinases (RLKs) are involved in plant growth, development, and immune responses and have undergone extensive expansion and diversification during plant evolution. However, comparative analyses of RLK subfamily expansion and duplication patterns across grasses have not been systematically integrated with analyses of RLK expression during oat leaf spot infection.

Methods: A unified hidden Markov model framework was used to identify and classify RLKs across 12 plant species and to analyze family expansion, duplication modes, and selection pressure. Time-series transcriptomes from resistant and susceptible oat accessions infected with *Drechslera avenae* were integrated with weighted gene co-expression network analysis (WGCNA) and expression screening to identify candidate AsaRLKs. Their evolutionary, regulatory, protein-structural, tissue-expression, and predicted-interaction features were then evaluated. Three selected genes were further examined by qRT-PCR following salicylic acid (SA) and methyl jasmonate (MeJA) treatments, with or without pathogen inoculation, and disease severity was assessed following hormone pretreatment.

Results: A total of 15870 RLKs were identified and assigned to 61 subfamilies. Oat contained 3039 RLKs, including 661 RLK_DLSV members; this subfamily had a relative expansion rate of 5.33. RLK gene pairs derived from whole-genome duplication (WGD) and tandem duplication (TD) were abundant and showed distinct distributions among species and subfamilies. Among 6209 WGD- and TD-derived gene pairs retained for Ka/Ks analysis, 6161 had Ka/Ks < 1, indicating that their coding sequences were predominantly subject to purifying selection. Intersection of 308 expression-

screened RLKs with 51 RLKs in the mediumorchid module yielded 29 candidates. Among the 29 candidates, *AsaRLK21* was the only Tier A gene, and it was prioritized alongside *AsaRLK27* and *AsaRLK28* based on their infection-responsive and tissue-expression profiles. The three genes exhibited distinct expression dynamics following SA and MeJA treatments. Both hormone pretreatments reduced disease incidence and disease index in the two oat accessions, with SA producing lower disease indices than MeJA.

Conclusions: Grass RLK families exhibited species- and subfamily-biased expansion, distinct duplication patterns, and predominantly purifying selection. Integrative analyses identified 29 candidate AsaRLK genes, with *AsaRLK21*, *AsaRLK27*, and *AsaRLK28* prioritized for further investigation, particularly *AsaRLK21*. These findings provide insights into RLK evolution and a basis for investigating oat leaf spot resistance.

Keywords: *Avena sativa*; receptor-like kinase; gene family evolution; gene duplication; *Drechslera avenae*; weighted gene co-expression network analysis

1 Introduction

Grasses are central to food and forage production, and oat (*Avena sativa* L.) is valued for its biomass, forage quality, and grain nutritional properties [1–7]. Oat leaf spot, caused in part by *Drechslera avenae*, produces foliar necrosis and reduces effective photosynthetic area, thereby threatening yield and quality [8,9]. Identifying the molecular components associated with contrasting oat responses to infection can help prioritize genetic resources for subsequent resistance studies.

Plants perceive microbe-associated molecules and damage signals through cell-surface pattern-recognition receptors (PRRs), whereas intracellular immune receptors recognize pathogen effectors

59 [10]. Although pattern-triggered immunity (PTI) and effector-triggered immunity (ETI) differ in the
60 location and type of receptor involved in recognition, they share downstream outputs such as protein
61 phosphorylation, changes in Ca^{2+} concentrations, reactive oxygen species (ROS) production,
62 mitogen-activated protein kinase (MAPK) cascades, and defence-gene expression [11,12]. The
63 receptor-like kinase (RLK) family is a major protein family that links extracellular signal perception
64 to intracellular phosphorylation. A typical RLK contains an extracellular region, a single
65 transmembrane region, and an intracellular protein kinase domain; its extracellular region may
66 contain leucine-rich repeat (LRR), lysin motif (LysM), lectin, wall-associated kinase (WAK),
67 CRINKLY4 (CR4), S-domain (SD), or domain of unknown function 26 (DUF26) modules [13,14].
68 Receptor-like proteins (RLPs) generally lack an intracellular kinase domain, whereas receptor-like
69 cytoplasmic kinases (RLCKs) usually lack a typical extracellular region and transmembrane region
70 and function primarily in cytoplasmic signalling downstream of receptor complexes [15–17]. Thus,
71 not every member of the RLK family is a membrane receptor with a complete extracellular region
72 and transmembrane region. Variation in the composition of extracellular, transmembrane, and
73 kinase regions provides a structural basis for diverse signal inputs and functional differentiation.

74 RLK family size and subfamily composition vary among plant lineages as a result of gene
75 duplication, loss, and differential retention [13,14]. Based on genomic location and collinearity,
76 duplicate relationships can be assigned to whole-genome duplication (WGD), tandem duplication
77 (TD), proximal duplication (PD), transposed duplication (TRD), and dispersed duplication (DSD)
78 classes [18]. WGD and TD have distinct genomic signatures, while the other duplication modes also
79 contribute to family composition and genome rearrangement [18,19]. Retained copies can
80 subsequently diverge in expression or coding sequence, making both duplication context and

sequence-level selective constraints informative for comparative analysis [20–23]. Grass lineages share an ancient ρ whole-genome duplication but differ in subsequent duplicate retention and loss [20]. The multiple subgenomes of wheat and cultivated allohexaploid oat add further complexity, and comparisons of cultivated and wild hexaploid oat genomes have revealed extensive chromosomal rearrangements [24–27]. These evolutionary processes provide a framework for comparing RLK subfamily composition and duplicate-gene evolution across grasses.

RLKs participate in pathogen perception and immune signalling through different receptor complexes and kinase-mediated pathways [13,17]. In *Arabidopsis thaliana* (*Ath*), flg22 promotes FLS2–BAK1 complex formation and defence activation [28]. In rice, OsCERK1 phosphorylates RLCK185, connecting chitin perception to a MAPK cascade [29]. In wheat, silencing *TaRLK2.4* increased susceptibility to *Blumeria graminis* f. sp. *tritici*, whereas overexpression enhanced resistance [30]. Knockout and overexpression experiments further linked *TaWAKL8-2B* with resistance to stripe rust and leaf rust and with linalool and ROS accumulation [31].

Existing resources, such as metaRLK and RLKdb, have provided comprehensive inventories and classification frameworks for RLKs across plant species, including oat [14,32]. In oat, Xiong et al. characterized the lectin receptor-like kinase family and investigated its responses to salt stress [33]. Previous studies have also documented physiological and transcriptional responses to oat leaf spot and powdery mildew, involving hormone signalling, phenylpropanoid metabolism, and immune-related pathways [9,34]. However, the evolutionary diversification and duplication patterns of RLK subfamilies across grasses remain incompletely understood, and the RLK members associated with contrasting responses of resistant and susceptible oat genotypes to *Drechslera avenae* infection have not been systematically characterized. Here, we compared RLKs across 10

grass species and two dicot reference species to investigate subfamily composition, relative expansion rates, duplication modes, and selective constraints. By integrating time-course transcriptomic data, weighted gene co-expression network analysis (WGCNA), and resistant–susceptible expression comparisons, we further prioritized candidate *Avena sativa* receptor-like kinase (AsaRLK) genes associated with leaf spot responses. The expression of three prioritized genes was subsequently examined under salicylic acid (SA) and methyl jasmonate (MeJA) treatments, alongside assessments of disease severity following hormone pretreatment. This study provides insights into RLK evolutionary diversification across grasses and establishes a basis for further investigation of candidate genes potentially involved in oat leaf spot resistance.

2 Materials and methods

2.1 Genome data sources and RLK identification

Genome datasets for 12 plant species were downloaded from public genome databases (Table S1). RLK genes were identified using HMMER hmmscan (version 3.4) [35]. Protein sequences were first searched against the Plant_Pkinase_fam hidden Markov model (HMM) library of the RLK/Pelle classification system. Candidate proteins with an E-value <1e-10 that could be assigned to an RLK subfamily were retained, and the best HMM hit was used for subfamily classification [36,37]. Proteins shorter than 250 amino acids were then removed, and completely redundant sequences were collapsed using CD-HIT (version 4.8.1) at a threshold of 100% sequence identity [38]. Candidate proteins were further searched against the Pfam domain models Pkinase (PF00069.31) and PK_Tyr_Ser-Thr (PF07714.23), and sequences with insufficient domain evidence were verified using InterProScan (version 5.77-108.0) [39–41]. Proteins without detectable kinase-domain evidence or with a kinase-domain alignment shorter than 100 amino acids were excluded.

125 The resulting high-confidence RLK genes were used in subsequent analyses.

126 **2.2 Phylogenetic, subfamily-expansion, and duplication-mode analyses**

127 RLK protein sequences identified in the 12 species were aligned using MAFFT, and the
128 alignment was trimmed with trimAl using the parameter -gt 0.2 [42,43]. The trimmed alignment
129 was used to construct a family-wide background tree for the 12 species with FastTree v2.2.0 under
130 the LG model (-lg -nosupport). The tree was annotated and visualized using iTOL [44,45].

131 To analyse RLK subfamily expansion and loss, RLK proteins from the 12 species were grouped
132 by subfamily and a gene tree was constructed for each subfamily. Sequences in each subfamily were
133 first aligned using MAFFT and trimmed with trimAl using -gt 0.2 [42,43]. For subfamilies with
134 fewer than 300 members, maximum-likelihood trees were constructed with IQ-TREE v3.0.1 under
135 the LG+G model (-fast -nt 4); gene trees for subfamilies with at least 300 members were constructed
136 with FastTree v2.2.0 under the LG model (-lg) [44,46]. Each subfamily gene tree was then
137 reconciled with the species tree inferred using OrthoFinder v2.5.5 in Notung v2.9.1.5. Under the
138 duplication–loss parsimony criterion, the root position with the lowest reconciliation cost was
139 selected, with costs of 1.5 and 1.0 assigned to gene-duplication and gene-loss events, respectively
140 [47,48]. The ancestral gene number for a subfamily was defined as the number of gene lineages
141 mapped to the root of the species tree, representing the most recent common ancestor of the 12
142 species. The relative expansion rate was calculated as the number of extant members of that
143 subfamily in a species divided by the inferred ancestral gene number.

144 **2.3 Duplication events and selection-pressure analysis**

145 Pairwise similarity searches of the retained RLK protein sequences were performed using
146 DIAMOND blastp (version 2.1.25) with an E-value threshold of 1e-5 [49]. DupGen_finder was then

used to classify duplicated gene pairs as WGD-, TD-, PD-, TRD-, or DSD-derived [18]. Only duplicated pairs in which both genes were RLKs were retained for RLK-specific duplication analysis. WGD- and TD-derived pairs were used for the principal analysis of duplication distributions and the subsequent analysis of selection pressure.

Selection pressure was further evaluated for WGD- and TD-derived RLK–RLK gene pairs. Protein sequences were aligned using the L-INS-i strategy in MAFFT (localpair --maxiterate 1000) [42]. Protein alignments were converted to codon alignments with PAL2NAL (version 14.1) and subsequently converted to AXT format [50]. Nonsynonymous substitution rates (Ka), synonymous substitution rates (Ks), and Ka/Ks ratios were calculated using KaKs_Calculator (version 2.0.1) under the GMYN model. Gene pairs satisfying $0 < Ks < 2$ and $0 \leq Ka/Ks \leq 10$ were retained for downstream analysis [51].

2.4 WGCNA and candidate RLK screening

To identify candidate RLK genes potentially involved in the oat leaf spot response, infection-expression data were extracted from a previously generated and publicly available transcriptome dataset from our group, deposited at the National Center for Biotechnology Information (NCBI) under BioProject PRJNA1470446 [52]. Weighted gene co-expression network analysis was performed on oat differentially expressed genes using the WGCNA R package. Genes with a mean fragments per kilobase of transcript per million mapped reads (FPKM) ≥1 and a coefficient of variation ≥0.5 were retained for network construction. A soft-thresholding power of $\beta=6$ was selected according to the scale-free topology criterion ($R^2 > 0.8$), and an unsigned weighted network was constructed. Modules were identified using the Dynamic Hybrid Tree Cut algorithm with a minimum module size of 30. Highly correlated modules were merged at $r > 0.75$, corresponding to

a merge cut height of 0.25 [53,54]. Kyoto Encyclopedia of Genes and Genomes (KEGG) enrichment analysis was conducted using the clusterProfiler R package (version 3.14.3). Enriched terms were ranked by significance, and the top 20 KEGG pathways were visualized [55,56].

Expression-based screening used the resistant/susceptible (R/S) infection time-course FPKM matrix generated by the sequencing provider's standard analysis, with the 3 biological replicates at each time point averaged. For each RLK gene, the maximum expression values in the resistant and susceptible accessions were calculated as R_max and S_max, respectively. Genes with max(R_max, S_max) ≤10 FPKM were excluded. Induction in the resistant accession was defined as R_fold ≥2 and R_max >10, where R_fold was the ratio of R_max to expression at 0 h post-inoculation (hpi) in the resistant accession. To avoid zero denominators, lower bounds of 1×10^{-6} and 0.01 were applied to R0 and S_max, respectively. Tier A was defined as R_max/S_max ≥2.0, and Tier B as 1.5 ≤ R_max/S_max <2.0. Tier C comprised genes that were neither Tier A nor Tier B but had expression in the resistant accession at least 1.2-fold higher than that in the susceptible accession at 3 or more time points, or satisfied R_fold ≥ 2 and R_max > 10.

2.5 Promoter elements and structural features

Chromosomal positions of oat RLK genes were extracted from the genome annotation, and their distributions across the 21 assembled chromosomes and unassembled scaffolds were summarized and visualized in Python. For each candidate gene, the 2-kb sequence upstream of the annotated 5′ end, accounting for strand orientation, was extracted as the promoter region, and cis-acting regulatory elements were predicted using PlantCARE [57]. Protein physicochemical properties were predicted using the ExPASy ProtParam online tool (https://www.expasy.org; accessed 23 January 2026) [58]. Protein domains were annotated using InterProScan (version 5.77-

191 108.0) [40,41]. Signal peptides were predicted using the SignalP 6.0 online server [59], and
192 transmembrane regions were predicted using the DeepTMHMM 1.0 online server
193 (https://services.healthtech.dtu.dk/services/DeepTMHMM-1.0/; accessed 5 March 2026).

194 **2.6 Candidate RLK expression profiles and predicted protein–protein interaction network**

195 Infection-expression analysis was based on the R/S infection time-course FPKM matrix
196 described above. For tissue-specific expression analysis, an oat RNA sequencing (RNA-seq) dataset
197 from the Plant Genomics and Phenomics Research Data Repository
198 (https://doi.org/10.5447/ipk/2022/2; accessed 1 March 2025) was used to obtain the tissue-
199 expression FPKM matrix.

200 Candidate AsaRLK proteins were mapped to homologous proteins in *Brachypodium*
201 *distachyon*, and oat protein associations were predicted by transferring homologous interaction
202 information from the Search Tool for the Retrieval of Interacting Genes/Proteins (STRING)
203 database. For each unordered oat protein pair obtained by homology transfer, the highest association
204 score was retained. First-neighbour predicted associations involving candidate AsaRLKs were
205 extracted, deduplicated, and visualized as a predicted protein–protein interaction (PPI) network
206 using Cytoscape.

207 **2.7 Hormone treatments, pathogen inoculation, and qRT-PCR analysis**

208 The leaf spot-resistant oat cultivar ‘Haymaker’ (R) and susceptible cultivar ‘Molasses’ (S)
209 were used as experimental materials. Seeds were treated with 75% ethanol for 30 s and 5% sodium
210 hypochlorite for 5 min, rinsed four times with sterile water, and soaked overnight. Seeds were sown
211 in a 1:1 (w/w) mixture of potting soil and vermiculite sterilized at 121°C for 20 min. Ten seeds were
212 sown per 10 × 10 × 20 cm cup and thinned to five seedlings one week after emergence. Plants were

grown under a 16 h light/8 h dark photoperiod at 22 ± 1°C during the day and 18 ± 1°C at night, with 65–75% relative humidity and a light intensity of 500–700 μmol m^{-2} s^{-1}.

Drechslera avenae was cultured on potato dextrose agar (PDA) at 28°C in the dark for 5 d. Ten 5-mm mycelial plugs from the colony margin were transferred to 100 mL of potato dextrose broth (PDB) and incubated at 28°C and 100 rpm in the dark for 5 d. The mycelia were collected, suspended in sterile 0.9% NaCl solution, and homogenized with two steel beads at 60 Hz for 180 s. The suspension was adjusted to 1 × 10^6 mycelial fragments mL^{-1} and supplemented with 0.2% Tween-80.

Fourteen-day-old seedlings were used for hormone and inoculation treatments. The hormone-response experiment included 100 μM SA, 100 μM MeJA, and a solvent control (CK), with leaves collected at 0, 1, 3, 6, 12, and 24 h after treatment. The inoculation experiment included CK, pathogen inoculation alone (D), SA pretreatment followed by inoculation (SA+D), and MeJA pretreatment followed by inoculation (MeJA+D). The corresponding hormones or solvent controls were applied 6 h before inoculation. Plants in the D, SA+D, and MeJA+D groups were then spray-inoculated with the pathogen suspension, while CK plants received pathogen-free inoculation solution. The inoculation time was designated 0 h post-inoculation (hpi), and leaves were collected at 0, 1, 3, 6, 12, 24, 48, and 72 hpi. Three biological replicates were established for each treatment at each time point, with three technical replicates per biological replicate.

Total RNA was extracted using a plant RNA extraction kit (TIANGEN Biotech, China) and reverse-transcribed into cDNA using the PrimeScript RT Reagent Kit (Takara Bio, Japan). Quantitative real-time PCR (qRT-PCR) was performed using SYBR Green Pro Taq HS Premix (Accurate Biology, China) on a Bio-Rad CFX96 Touch system (Bio-Rad, USA). Primer sequences

are listed in Table S2. *Actin* was used as the reference gene, and relative expression levels were calculated using the 2^−ΔΔCt method. For the hormone-response experiment, CK at 0 h for each gene in each cultivar was used as the calibrator, whereas the corresponding time-matched CK was used for the inoculation experiment. Results were expressed as mean ± standard deviation (SD).

Disease severity was assessed at 7 d post-inoculation. Each inoculation treatment included eight independent biological replicates, with 30 leaves evaluated per replicate. Disease incidence and disease index were calculated according to a 0–4 disease severity scale (Table S3).

$$\text{Diseased leaf rate} = \frac{\text{Number of diseased leaves}}{\text{Total number of leaves assessed}} \times 100\%$$

$$\text{Disease index} = \frac{\sum(\text{Number of leaves at each disease grade} \times \text{corresponding disease grade})}{\text{Total number of leaves assessed} \times \text{highest disease grade}} \times 100$$

2.8 Statistical analysis

Data processing was performed using R and Python, with basic descriptive statistics calculated in Microsoft Excel 2021. Figures were generated using R packages and Python. One-way ANOVA followed by Tukey's HSD multiple comparison test ($P<0.05$) was applied to compare relative expansion rates among RLK subfamilies and disease incidence and disease index among treatment groups. For RLK expansion analysis, all 61 subfamilies were compared using their relative expansion rates across 12 species, although only the top 20 subfamilies were displayed in Fig. 1B and C. For disease assessment, six cultivar–treatment groups were compared separately for each disease metric, with eight independent biological replicates per group (Fig. 8K, L).

3 Results

3.1 Identification, classification, and expansion of RLK genes

A total of 15870 RLK members were identified from 12 plant species, comprising 2 dicots and 10 grasses. These genes were assigned to 61 RLK subfamilies (Fig. 1A; Table S4). RLK family size varied markedly among species, ranging from 621 to 3895 members across all 12 species and from 846 to 3895 members among the 10 grasses. Across the dataset, RLK_DLSV was the largest subfamily, with 2907 members. *Solanum lycopersicum* (*Sly*) had the fewest RLK members (621), followed by *Ath* (624). Other large subfamilies included RLK_WAK (1363 members), RLK_L-LEC (1242), RLK_SD-2b (1207), and RLK_LRR-XII-1 (1103). RLK_RLCK-Os was restricted to grasses, whereas RLK_RLCK-XII-2, RLK_Singleton, RLK_DSLV, and RLK_RLCK-XVII were absent from the grass species and had few members in *Ath* and *Sly*. These patterns indicated extensive diversification in RLK family size among plants, including within grasses. A phylogenetic tree was subsequently constructed from the identified RLK protein sequences (Fig. S1). Most RLK members clustered broadly according to subfamily, and the overall tree topology was broadly consistent with the best-HMM-hit-based subfamily assignments.

Relative expansion rates were subsequently calculated for each subfamily, revealing distinct subfamily- and species-specific variation (Fig. 1B, C; Table S5). RLK_RLCK-Os, RLK_LRR-XII-1, RLK_WAK, RLK_LRK10L-2, and RLK_DLSV showed high mean relative expansion rates (Fig. 1B). *Triticum aestivum* (*Tae)* and *Asa* showed pronounced expansion across several major RLK subfamilies. In addition to these two species, RLK_LRR-XII-1 also showed high expansion rates in *Setaria italica* (*Sit*), *Lolium perenne* (*Lpe*), *Sorghum bicolor* (*Sbi*), *Oryza sativa* (*Osa)*, and *Brachypodium distachyon* (*Bdi*), whereas RLK_WAK was prominently expanded in *Sit*, *Lpe*,

Hordeum vulgare (*Hvu)*, *Sbi*, and *Osa* (Fig. 1C). RLK_LRK10L-2 showed varying degrees of expansion in *Tae*, *Sbi*, *Hvu*, and *Osa*, whereas RLK_DLSV was markedly expanded in both *Tae* and *Asa*. RLK_RLCK-Os showed high expansion rates in grass species including *Asa*, *Hvu*, *Bdi*, *Zea mays* (*Zma)*, *Sbi*, *Lpe*, and *Panicum hallii* (*Pha*) (Table S5). Overall, RLK family expansion was not uniform across subfamilies or species, but showed clear subfamily bias and species specificity.

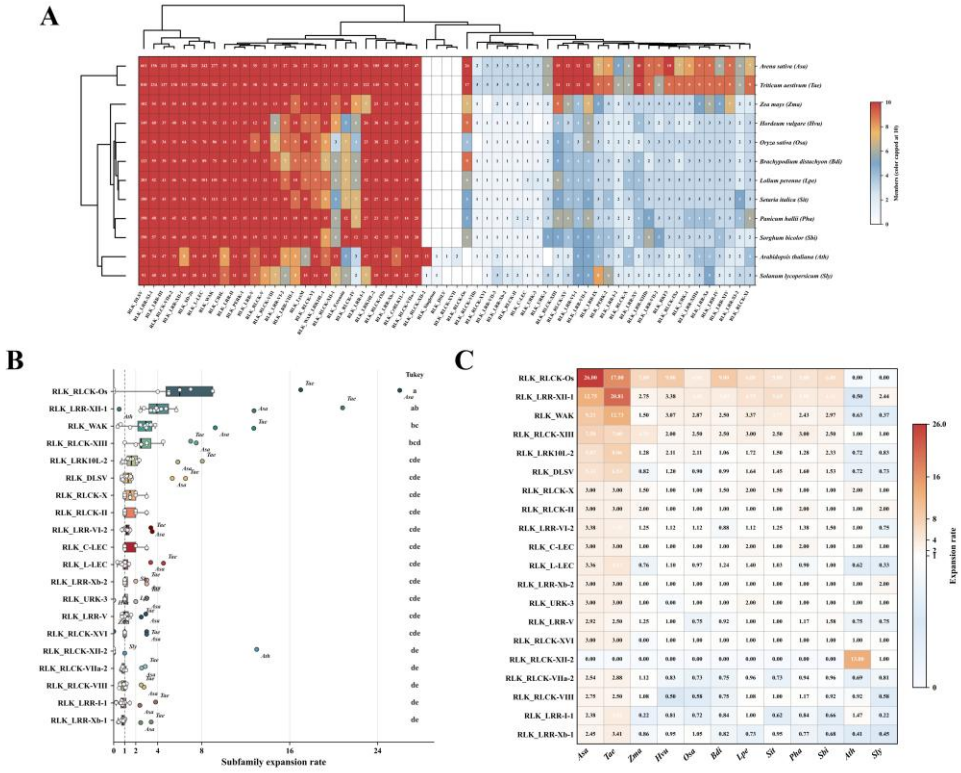


Figure 1 Identification, classification, and expansion of receptor-like kinase (RLK) genes in 12 species. (A) Heatmap showing the number of members in each RLK subfamily across the 12 species. (B) Only the 20 RLK subfamilies with the highest mean relative expansion rates across the 12 species are shown; different lowercase letters indicate significant differences based on comparisons among all 61 subfamilies (adjusted P<0.05). (C) Heatmap showing relative expansion rates across the 12 species for the same 20 RLK subfamilies shown in (B).

3.2 WGD- and TD-derived RLK gene pairs were unevenly distributed across species and

subfamilies

Across the 12 species, 27243 duplicated RLK gene pairs were identified, comprising 6406 WGD-, 2518 TD-, 1280 PD-, 1933 TRD-, and 15106 DSD-derived pairs (Table S6). DSD-derived pairs were the most numerous, followed by WGD- and TD-derived pairs.

The abundance of duplicated gene pairs differed markedly among plant species and RLK subfamilies (Fig. 2A, B; Table S6). Absolute counts of WGD- and TD-derived pairs were highest in polyploid grasses: *Tae* and *Asa* contained 2648 and 2272 WGD-derived pairs, respectively, and 643 and 439 TD-derived pairs. By contrast, diploid grasses and the two dicot reference species generally contained fewer WGD- and TD-derived pairs, showing that polyploid grasses contained more such RLK pairs in absolute terms. Duplicated-pair abundance also varied among RLK subfamilies (Fig. 2B–D; Table S6). When WGD- and TD-derived pairs were considered together, RLK_DLSV had the largest number of duplicated pairs, with 1468 in total, including 714 TD- and 754 WGD-derived pairs. RLK_L-LEC, RLK_WAK, RLK_SD-2b, RLK_RLCK-VIIa-2, and RLK_LRR-XII-1 also contained large numbers of duplicated pairs. Thus, high absolute counts of WGD- and TD-derived pairs were concentrated in a subset of RLK subfamilies rather than distributed uniformly across the family.

In the species-by-subfamily matrices, WGD- and TD-derived pair counts ranged from 0 to 336 and from 0 to 170, respectively (Fig. 2C, D; Table S6). Within RLK_DLSV, 285 WGD- and 109 TD-derived pairs were detected in *Asa*, compared with 336 WGD- and 170 TD-derived pairs in *Tae*. RLK_L-LEC, RLK_WAK, and RLK_SD-2b also contained both WGD- and TD-derived pairs. Overall, WGD-derived pairs were broadly distributed across numerous RLK subfamilies, whereas TD-derived pairs were more concentrated in a subset of subfamilies, including RLK_DLSV,

RLK_L-LEC, RLK_WAK, RLK_SD-2b, RLK_LRR-XII-1, and RLK_LRK10L-2. Both pair types were abundant but showed distinct distributions among species and subfamilies.

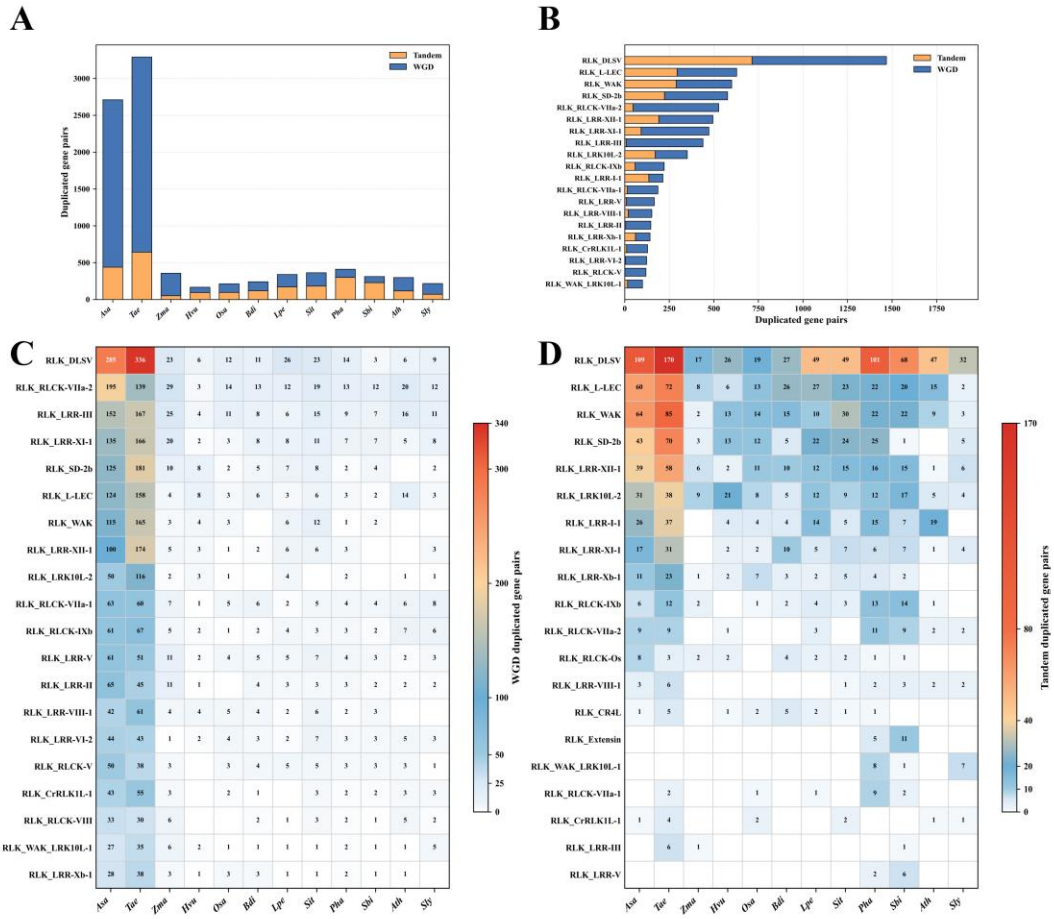


Figure 2 Distribution of whole-genome duplication (WGD)- and tandem duplication (TD)-derived RLK gene pairs in 12 species. (A, B) Numbers of WGD- and TD-derived pairs across species (A) and RLK subfamilies (B). (C, D) Heatmaps showing the numbers of duplicated pairs in RLK subfamilies across the 12 species, with WGD-derived pairs in (C) and TD-derived pairs in (D). Only the top 20 subfamilies in each analysis are shown in (B–D).

3.3 Retained WGD- and TD-derived RLK gene pairs were predominantly subject to purifying

selection

The Ka/Ks analysis retained 4473 WGD-derived and 1736 TD-derived gene pairs (Fig. 3A, B; Table S7). Of these, 6161 pairs had Ka/Ks <1 and 48 had Ka/Ks >1, indicating predominantly purifying selection on their coding sequences. The median Ka/Ks ratio was lower for WGD-derived pairs than for TD-derived pairs (0.173029 versus 0.288909).

In oat, 2061 gene pairs passed the Ka/Ks filters, of which 2046 had Ka/Ks < 1 (Fig. 3A, B). This oat subset comprised 1737 WGD-derived and 324 TD-derived pairs, with median Ka/Ks ratios of 0.159607 and 0.2551645, respectively. Consistent with the multispecies background, the coding sequences of the retained WGD- and TD-derived oat RLK pairs were predominantly subject to purifying selection.

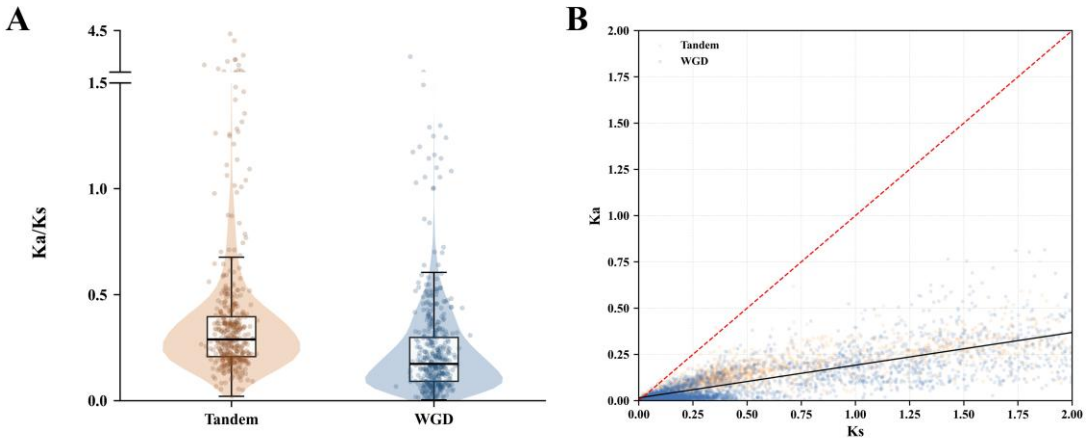


Figure 3 Selection analysis across the 12 species. (A) Distribution of Ka/Ks ratios for WGD- and TD-derived gene pairs. (B) Scatter plot of Ka and Ks for duplicated RLK gene pairs. The red dashed line indicates Ka=Ks, and the black solid line represents the linear regression trend between Ka and Ks.

3.4 Genome-wide chromosomal distribution of oat RLK subfamilies

Of the 3039 oat RLK genes assigned to 57 subfamilies, 2972 were located on the 21 assembled chromosomes and 67 on unassembled scaffolds (Fig. 4). The numbers of anchored RLK genes varied among chromosomes, with relatively large counts on 2D (198), 2A (186), 5D (178), 6A (161), 1D (160), 6C (159), 3C (155), and 7D (153).

Chromosome-anchored RLK genes were concentrated in several large subfamilies. RLK_DLSV was the largest, with 643 genes on the 21 assembled chromosomes and a further 18 members on unassembled scaffolds. Other abundant chromosome-anchored subfamilies included RLK_WAK (274 members), RLK_L-LEC (238), RLK_SD-2b (223), RLK_LRR-XII-1 (199), RLK_LRR-XI-1 (153), RLK_RLCK-VIIa-2 (121), and RLK_LRR-III (117).

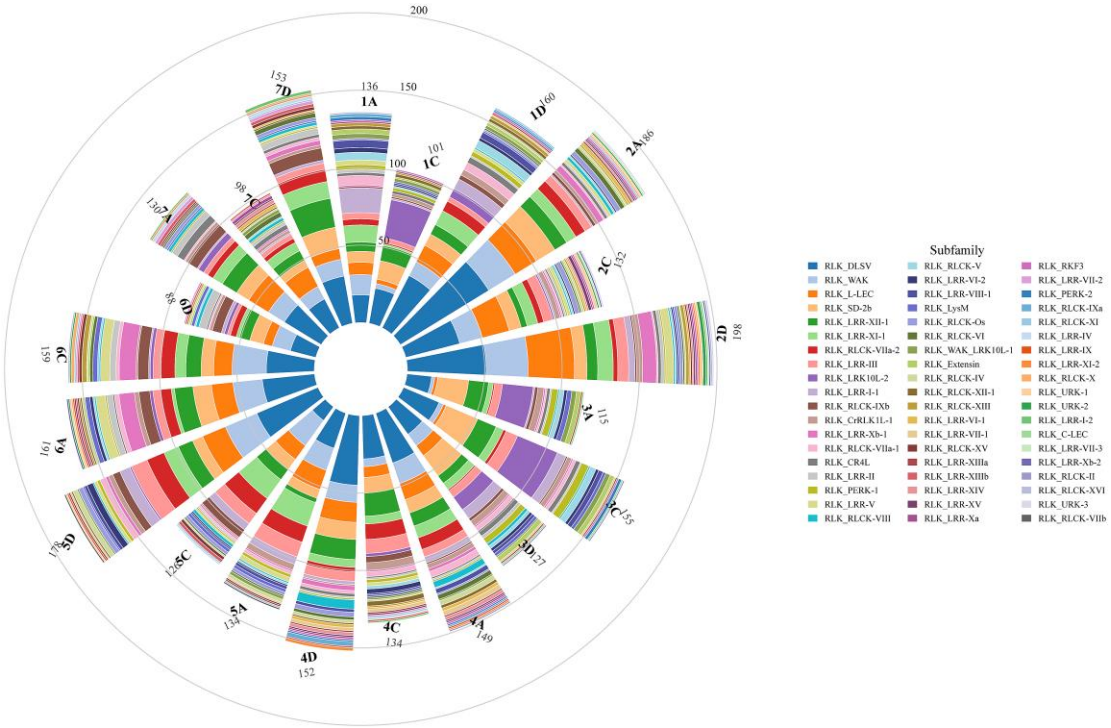


Figure 4 Chromosomal distribution of oat RLK subfamilies across the 21 assembled chromosomes.

3.5 WGCNA and expression screening jointly identified 29 candidate RLK genes

WGCNA of the oat leaf spot infection time-course dataset (NCBI BioProject PRJNA1470446)

identified a mediumorchid module containing 743 genes, including 51 RLKs (Fig. 5A; Table S8). The module showed positive associations with early infection time points in both resistant and susceptible oat accessions. KEGG enrichment identified plant–pathogen interaction, MAPK signalling pathway–plant, and plant hormone signal transduction among its enriched pathways (Fig. 5B). The module was therefore used as the co-expression component of candidate RLK screening.

Expression-based screening was then integrated to define the candidate RLK set. Among oat RLK genes represented in the infection time-course expression matrix, 308 passed the A/B/C expression-screening criteria (Table S8). Intersecting these 308 expression-screened RLKs with the 51 RLKs in the mediumorchid module yielded 29 candidate RLK genes. The 29 candidates comprised 1 Tier A gene, 1 Tier B gene, and 27 Tier C genes. RLK_DLSV was the most abundant subfamily in the candidate set, with 8 genes, followed by RLK_RLCK-VIIa-2 with 6 and RLK_CR4L with 3; the remaining subfamilies were represented by 1 or 2 genes each.

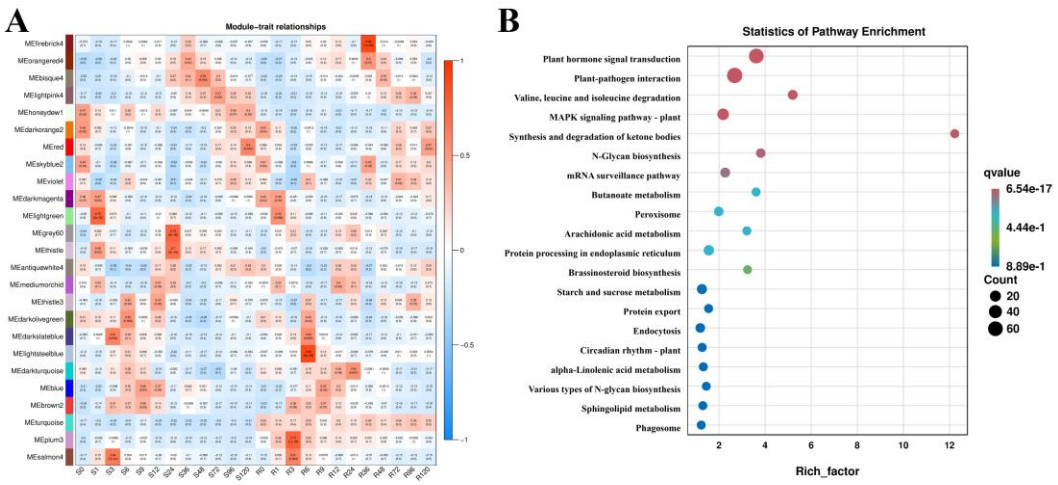


Figure 5 Candidate RLK screening using weighted gene co-expression network analysis (WGCNA) and Kyoto Encyclopedia of Genes and Genomes (KEGG) enrichment analysis. (A) Heatmap of correlations between WGCNA modules and infection time points in resistant and susceptible oat accessions. (B) KEGG enrichment bubble plot for genes in the mediumorchid module.

3.6 Chromosomal locations, promoter elements, and protein features of the 29 candidate AsaRLK genes

The 29 candidate RLK genes were distributed across 17 assembled oat chromosomes. Within this candidate set, 18 genes were connected by 12 identified WGD-derived pairs, forming 8 WGD-connected groups (Fig. S2). For display purposes, the candidates were designated *AsaRLK1*–*AsaRLK29* according to chromosomal order.

Promoter cis-element prediction identified hormone- and stress-related motifs across the 29 candidate AsaRLK promoters (Fig. 6). MeJA- and abscisic acid (ABA)-responsive elements were widespread, whereas SA-responsive elements were less frequent. Light-responsive, MYB-related drought-responsive, low-temperature-responsive, gibberellin-responsive, meristem-expression-related, and circadian-regulatory elements were also detected. *AsaRLK28* and *AsaRLK23* had relatively high numbers of predicted MeJA- and SA-responsive elements, respectively, and both contained multiple ABA-responsive elements. The *AsaRLK21* promoter contained 10 predicted MeJA-responsive and 2 SA-responsive elements, together with MYB-related drought- and light-responsive motifs.

To describe the basic properties of the 29 candidate AsaRLK proteins, we calculated their amino-acid length, molecular weight, theoretical isoelectric point, instability index, aliphatic index, and hydropathicity (Table S9). The 29 proteins ranged from 293 to 1068 amino acids, with molecular weights of 32.013–116.431 kDa and theoretical isoelectric points of 5.651–9.800. Most candidate proteins had grand average of hydropathicity (GRAVY) values below 0, indicating an overall hydrophilic character. Protein-domain architecture analysis showed that all 29 candidate RLK proteins contained kinase-related domains, but differed in their extracellular domains, signal

peptides, and transmembrane regions (Fig. S3). AsaRLK28 contained a signal peptide, an LRR domain, a transmembrane region, and a protein kinase domain, consistent with the architecture of a typical membrane-localized RLK. By contrast, AsaRLK21 contained only a detectable protein kinase domain and lacked a typical extracellular receptor domain and transmembrane region, more closely resembling an intracellular RLCK. Overall, the 29 candidates differed in promoter elements, physicochemical properties, and protein-domain architecture, indicating regulatory and structural diversity among candidate AsaRLK members.



Figure 6 Distribution of cis-acting elements in the promoters of the 29 candidate *Avena sativa* receptor-like kinase (*AsaRLK*) genes.

3.7 Expression profiles and predicted protein associations of candidate AsaRLK genes

The 29 candidate RLK genes exhibited distinct expression patterns during oat leaf spot infection, with expression peaks predominantly occurring at 1, 12, and 24 hpi (Fig. 7A). Among

401 them, *AsaRLK27* showed relatively high expression during the early infection stage, while
402 *AsaRLK24*, *AsaRLK8*, *AsaRLK17*, *AsaRLK22*, and *AsaRLK28* exhibited increased expression at
403 different time points. *AsaRLK21*, the only Tier A candidate, showed higher expression in the
404 resistant cultivar than in the susceptible cultivar at 1, 12, and 24 hpi. Tissue-specific expression
405 analysis revealed distinct expression profiles among the candidate RLK genes (Fig. 7B). *AsaRLK21*
406 exhibited the highest expression in roots, *AsaRLK27* was highly expressed in crowns and glumes,
407 and *AsaRLK12* maintained relatively high expression in crowns, panicles, and seeds. *AsaRLK28*
408 showed higher expression in panicles and seeds, while *AsaRLK4* and *AsaRLK6* were highly
409 expressed in multiple reproductive tissues.

410 A first-neighbour predicted protein association network was constructed for the 29 candidate
411 AsaRLKs by transferring homologous STRING association data from *Brachypodium distachyon*
412 (Fig. 7C). The resulting network contained 4426 nodes and 26793 edges, including 29 candidate
413 nodes and 4397 first-neighbour nodes. Predicted connectivity differed among candidates: several
414 RLK_DLSV proteins, including AsaRLK7, AsaRLK8, AsaRLK10, AsaRLK13, AsaRLK18, and
415 AsaRLK21, occurred in densely connected regions. Direct predicted associations among the 29
416 candidates were relatively few; most edges linked candidates to first-neighbour proteins. These
417 patterns distinguish the candidates by their transferred association profiles and provide specific
418 predicted connections for subsequent testing.

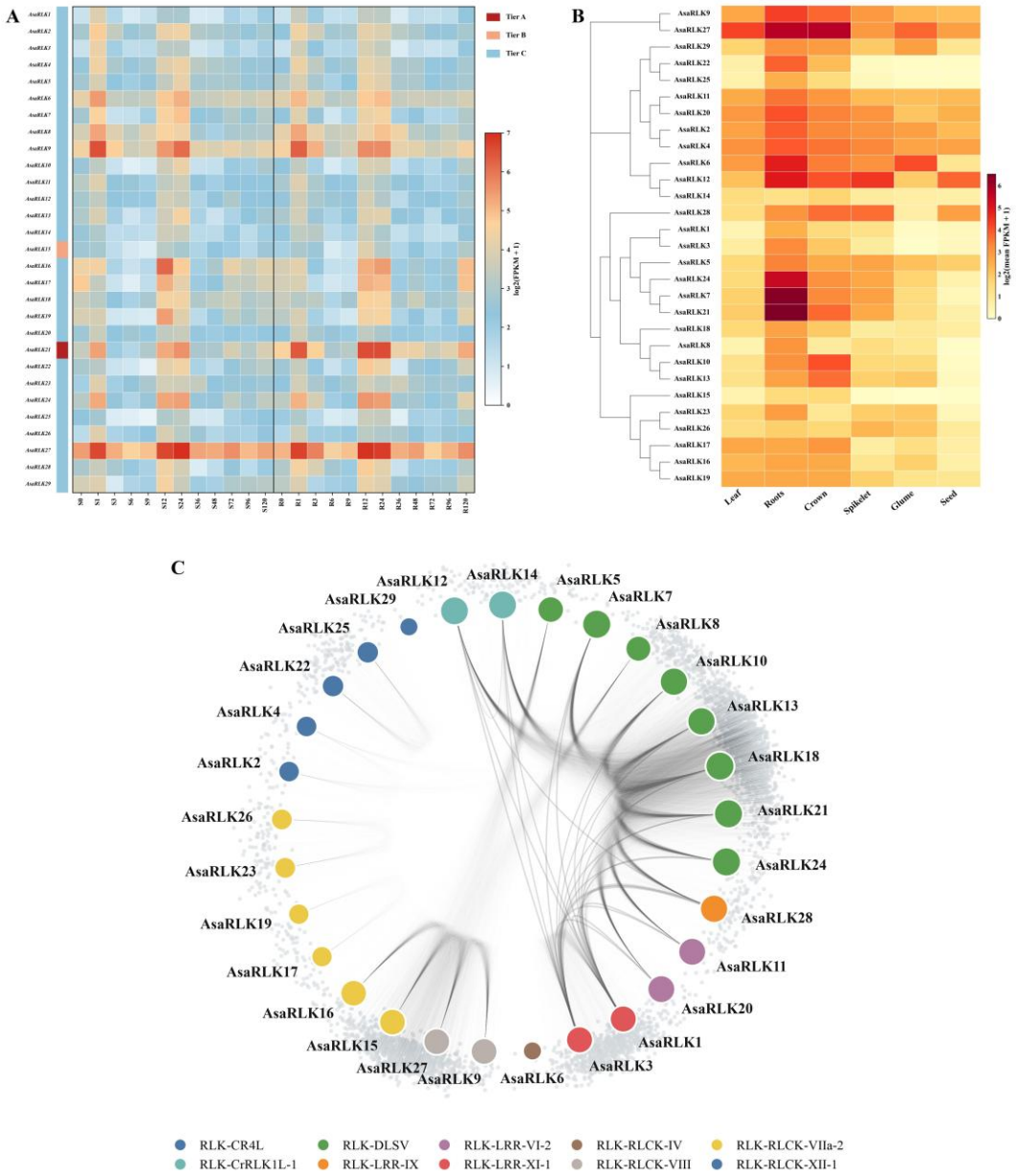


Figure 7 Expression patterns and predicted protein–protein interaction (PPI) network of the 29 candidate *AsaRLK* genes. (A) Heatmap showing the expression of the 29 candidate *AsaRLK* genes during oat leaf spot infection in resistant and susceptible accessions. (B) Heatmap showing the expression of the 29 candidates in leaves, roots, crowns, panicles, floret glumes, and seeds. (C) Predicted first-order protein–protein interaction (PPI) network of 29 candidate AsaRLK proteins constructed through interolog-based interaction transfer using STRING data from *Brachypodium distachyon*. R, resistant accession; S, susceptible accession.

3.8 Hormone-responsive expression of candidate AsaRLK genes and associated disease phenotypes

The three candidate genes, *AsaRLK21*, *AsaRLK27*, and *AsaRLK28*, exhibited distinct expression dynamics in response to SA and MeJA treatments, with differences observed between the two oat cultivars (Fig. 8A–I). In the absence of pathogen inoculation, the relative expression levels of *AsaRLK21* and *AsaRLK27* in Haymaker reached 5.31 and 4.19 at 1 h after SA treatment, respectively, exceeding those of the corresponding CK groups (1.61 and 1.44). *AsaRLK28* exhibited a transient expression peak at 1 h across all treatments. Following inoculation, all three genes in Haymaker reached peak expression at 6 hpi in the pathogen-only treatment (D), with relative expression levels of 17.18, 14.25, and 9.82, respectively, exceeding those in the corresponding SA+D and MeJA+D groups. In Molasses, *AsaRLK21* and *AsaRLK27* peaked at 12 hpi under SA+D treatment (19.44 and 15.00, respectively), whereas their expression peaks under MeJA+D treatment occurred at 24 hpi (10.48 and 12.22, respectively). Both hormone pretreatments alleviated leaf spot symptoms (Fig. 8J–L). In Haymaker, the diseased leaf incidence rates under D, MeJA+D, and SA+D treatments were 21.67%, 14.58%, and 12.08%, respectively, with corresponding disease indices of 9.58, 6.35, and 3.02. In Molasses, the corresponding diseased leaf incidence rates were 75.83%, 40.00%, and 25.83%, with disease indices of 45.21, 23.33, and 11.88, respectively.

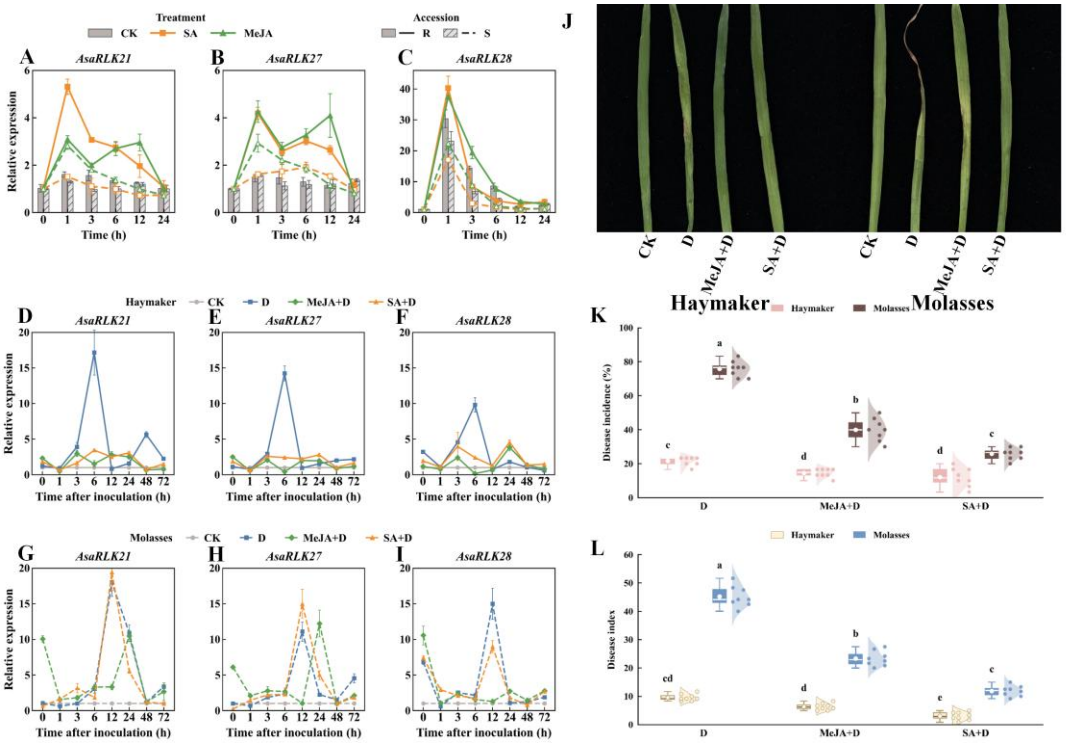


Fig. 8. Hormone-responsive expression of candidate AsaRLK genes and associated disease phenotypes. (A–C) Relative expression levels of *AsaRLK21*, *AsaRLK27*, and *AsaRLK28* under CK, SA, and MeJA treatments without pathogen inoculation, normalized to CK at 0 h for each gene in each cultivar. Data are presented as mean ± SE. (D–F) Expression dynamics of the three genes under CK, D, MeJA+D, and SA+D treatments in Haymaker (R) and (G–I) Molasses (S), normalized to the corresponding CK at each time point using *Actin* as the reference gene. Data are presented as mean ± SE. (J) Representative leaf symptoms under different treatments. (K) Disease incidence and (L) disease index. CK, control; D, pathogen inoculation alone; SA, salicylic acid; MeJA, methyl jasmonate; SA+D and MeJA+D, pathogen inoculation following 6 h of SA or MeJA pretreatment, respectively.

4 Discussion

4.1 Divergence in RLK composition and subfamily-specific expansion across grasses

Polyploidization increases the number of gene copies available for retention, but subsequent losses and unequal retention shape the extant RLK repertoire [60–62]. Yan et al. reported widespread retention of homoeologous RLKs across the A, B, and D subgenomes of wheat and its relatives [63]. Using gene-tree/species-tree reconciliation, collinearity, and Ks analyses across 363 grasses, Zhang et al. showed that lineages sharing the ancient ρ WGD nevertheless retained different proportions of duplicated genes [20]. In our dataset, both wheat and oat contained large RLK families and showed high relative expansion rates, but the most expanded subfamilies and their expansion levels differed between the two species (Fig. 1A–C; Tables S4, S5).

Oat genomic studies reveal variation in RLK composition across ploidy levels and genetic backgrounds. Xiong et al. found more LecRLKs in cultivated hexaploid oat than in tetraploid *Avena insularis* or diploid *Avena longiglumis*, together with uneven chromosomal distributions and distinct stress-responsive expression patterns [33]. Avni et al. identified extensive variation in gene content, genome structure, and expression among 33 wild and cultivated hexaploid oat accessions [25]. Our reference-genome analysis likewise detected unequal numbers of RLK genes among chromosomes and subfamilies (Fig. 4; Table S4).

The distribution of RLK subfamilies differed not only in copy number but also between the grass and dicot reference lineages. Gawande and Sankaranarayanan identified 15 CrRLK1L genes in wheat and reported variation in their tissue-, developmental-, and stress-associated expression [64]. In a survey covering 528 plant species, Liu et al. detected RLCK-XVII and RLCK-XII-2 only in dicots [14], consistent with the absence of these subfamilies from the 10 grasses analysed here

(Fig. 1A; Table S4). By contrast, RLK_RLCK-Os occurred in the grass species and not in the two dicot references. RLK_RLCK-Os, RLK_LRR-XII-1, RLK_WAK, RLK_RLCK-XIII, RLK_LRK10L-2, and RLK_DLSV also showed high mean relative expansion rates in the 12-species comparison (Fig. 1B, C; Table S5). The contrasting distributions identify lineage-associated differences in RLK subfamily representation, alongside pronounced variation in expansion among individual grass species.

4.2 Distribution and selective constraints of different RLK duplication modes

Qiao et al. reported that WGD-, TRD-, and DSD-derived pair counts declined with duplication age, whereas TD and PD did not show the same significant pattern [18]. In seven representative grasses, Chen et al. identified WGD-, DSD-, and TRD-derived relationships in the TLP family, with DSD being the most numerous [19]. DSD-derived pairs were also the largest class in our RLK–RLK dataset (Table S6).

Duplication modes were distributed unevenly among RLK subfamilies. Yan et al. identified 232 tandemly duplicated RLK clusters in wheat, with the largest and second-largest clusters both belonging to the RLK_DLSV subfamily [63]. Consistent with this pattern, our within-subfamily dataset contained 6038 WGD- and 2479 TD-derived pairs, spanning 57 and 45 RLK subfamilies, respectively. TD-derived pairs in RLK_DLSV, RLK_L-LEC, and RLK_WAK together accounted for 52.3% of all within-subfamily TD-derived pairs, whereas the corresponding proportion among within-subfamily WGD-derived pairs was 23.2%. WGD-derived relationships thus extended across a broader range of subfamilies, while TD-derived relationships were more strongly concentrated in particular subfamilies (Fig. 2B–D; Table S6).

The generally low Ka/Ks values suggest that coding-sequence constraint can coexist with variation in duplicated-gene expression. Qiao et al. found purifying selection alongside decreasing expression correlations among duplicated genes over evolutionary time [18]. Ezoe et al. also reported differences in selective pressure among stages of wheat polyploidization [65]. These comparisons support examining coding-sequence conservation and expression divergence as separate features of retained duplicates. The WGD-linked oat candidates in Fig. S2 provide defined groups for such expression comparisons.

4.3 Disease-responsive candidate RLKs identified through co-expression and infection-expression screening

Functional studies have linked several RLK classes to resistance against fungal pathogens in grasses [30]. In wheat, *Stb16q* and *Stb15* encode a cysteine-rich RLK and a G-type lectin RLK, respectively. While *Stb16q* restricts the penetration and intercellular growth of *Zymoseptoria tritici* and confers broad-spectrum resistance, *Stb15* mediates isolate-specific resistance [66,67]. The G-type lectin RLK TaSRLK interacts with and phosphorylates TaPrx1, promoting ROS-associated resistance to stripe rust [68]. Resistance to *Rhizoctonia cerealis* also involves TaCRK3, which exhibits DUF26-dependent antifungal activity and regulates ethylene-associated defence gene expression [69]. Another wheat kinase, TaWAK-6D, promotes defence gene expression and contributes to resistance against both *Fusarium pseudograminearum* and *R. cerealis* [70]. In maize, the WAK-type kinase Htn1 slows the development of northern corn leaf blight caused by *Setosphaeria turcica* [71], whereas rice OsSRF3 contributes to OsBAK1-associated antifungal immune signalling [72]. The diversity of RLK structures and defence-related activities reported in

these studies provides a rationale for examining infection-responsive expression and co-expression patterns when prioritizing candidate RLKs in oat.

The mediumorchid module captured a shared early infection-associated expression pattern in resistant and susceptible oat accessions (Fig. 5A). Its enrichment in plant–pathogen interaction, MAPK signalling, and hormone signal transduction placed the selected RLKs within a defence-related co-expression context (Fig. 5B). Intersecting module membership with the expression criteria selected 29 RLKs that combined temporal coordination with sufficient expression and induction in the resistant accession. Network- and expression-based prioritization has also been applied in pepper, poplar, and wheat [73–75]. In pepper, VIGS identified immune or disease-resistance phenotypes in a subset of the network-selected RLPs [73].

Among the 29 candidates, *AsaRLK21*, *AsaRLK27*, and *AsaRLK28* were selected for further investigation based on their infection-responsive expression patterns and supporting gene-level evidence. *AsaRLK21* was classified as a Tier A candidate and exhibited early R-biased expression, whereas *AsaRLK27* showed an early infection response. The predicted membrane-receptor architecture of *AsaRLK28* provided additional structural context for its selection. SA- and MeJA-responsive cis-regulatory elements in their promoters provided a rationale for examining the effects of these hormones. Both pretreatments reduced disease indices in the resistant and susceptible oat accessions, with SA producing lower values than MeJA (Fig. 8K, L). Koley et al. reported a similar pattern in tomato infected with *Rhizoctonia solani*, where SA pretreatment resulted in a lower disease index than MeJA [76]. In wheat, however, Dinolfo et al. observed cultivar-dependent effects of MeJA on *Fusarium poae* infection [77]. Gao et al. further found that MeJA-mediated suppression of *Fusarium graminearum* infection was primarily associated with inhibition of fungal toxin

biosynthesis rather than enhanced host defence gene expression [78]. In Haymaker, pathogen inoculation alone produced higher peak expression of the three candidate RLKs than SA or MeJA pretreatment followed by inoculation.

5 Conclusion

Together, these findings reveal distinct duplication-associated evolutionary patterns and predominantly purifying selection shaping RLK diversification across grasses. In oat, the integration of infection-responsive expression, resistant–susceptible comparisons, and co-expression analysis identified 29 candidate RLKs, with *AsaRLK21* emerging as the sole Tier A candidate. The distinct SA- and MeJA-responsive expression patterns of *AsaRLK21*, *AsaRLK27*, and *AsaRLK28*, together with the reduced disease severity following hormone pretreatment, highlight the potential relevance of hormone-associated RLK responses to oat leaf spot resistance. More broadly, this study connects RLK evolutionary diversification with pathogen-responsive expression, providing a foundation for investigating disease-associated signaling and prioritizing candidate resistance-related genes in polyploid crops.

Supporting information

Table S1, Genome assemblies and data sources for 12 plant species; Table S2, Primer sequences used for qRT-PCR analysis of *AsaRLK21*, *AsaRLK27*, and *AsaRLK28*; Table S3, Classification standard for oat leaf spot disease severity; Table S4, Identification and subfamily classification of RLK proteins in 12 plant species; Table S5, RLK subfamily sizes and relative expansion rates across 12 plant species; Table S6, Five RLK gene duplication modes and distributions of WGD- and TD-derived gene pairs; Table S7, Ka/Ks analysis of filtered WGD- and TD-derived RLK gene pairs; Table S8, WGCNA and expression evidence for candidate RLK

screening; Table S9, Physicochemical properties of the 29 candidate AsaRLK proteins. Fig. S1, Phylogenetic overview and subfamily distribution of 15870 RLK proteins from 12 plant species; Fig. S2, Chromosomal locations and WGD relationships among the 29 candidate AsaRLK genes; Fig. S3, Phylogenetic relationships and predicted domain architectures of the 29 candidate AsaRLK proteins.

Authors' contributions

G.Q.Z. conceived and supervised the study. Y.N.C., K.J.N., and J.K.C. performed the experiments and acquired the data. Y.N.C., L.Z., W.P.W., Y.M.M., and P.P.H. analyzed the data and drafted the manuscript. G.Q.Z. and K.J.N. revised the manuscript. All authors read and approved the final manuscript.

Funding

This work was supported by the National Natural Science Foundation of China (32360342) and the China Agriculture Research System (CARS-07-C-1).

Data availability

Raw oat leaf spot infection RNA-seq data have been deposited in the NCBI BioProject database under accession number PRJNA1470446. The publicly available oat tissue-expression dataset used in this study was obtained from the Plant Genomics and Phenomics Research Data Repository under DOI: 10.5447/ipk/2022/2. All other data generated or analysed during this study are included in this published article and its supplementary information files.

Acknowledgments

We sincerely thank the Pratacultural College, Gansu Agricultural University, and the Key Laboratory of Grassland Ecosystems, Ministry of Education, for providing experimental facilities

and technical support.

Declarations

Ethics approval and consent to participate

Not applicable.

Consent for publication

Not applicable.

Competing interests

The authors declare no competing interests.

References

1. Cheng A, Mohd Hanafiah N, Harikrishna JA, Eem LP, Baisakh N, Mispan MS. A reappraisal of polyploidy events in grasses (Poaceae) in a rapidly changing world. Biology. 2022;11:636. https://doi.org/10.3390/biology11050636.

2. Kellogg EA. Relationships of cereal crops and other grasses. Proc Natl Acad Sci U S A. 1998;95:2005–10. https://doi.org/10.1073/pnas.95.5.2005.

3. Linder HP, Lehmann CER, Archibald S, Osborne CP, Richardson DM. Global grass (Poaceae) success underpinned by traits facilitating colonization, persistence and habitat transformation. Biol Rev Camb Philos Soc. 2018;93:1125–44. https://doi.org/10.1111/brv.12388.

4. Ji Y, Hewavithana T, Sharpe AG, Jin L. Understanding grain development in the Poaceae family by comparing conserved and distinctive pathways through omics studies in wheat and maize. Front Plant Sci. 2024;15:1393140. https://doi.org/10.3389/fpls.2024.1393140.

5. Hanoğlu Oral H. Forage yields and nutritive values of oat and triticale pastures for grazing sheep in early spring. PeerJ. 2024;12:e17840. https://doi.org/10.7717/peerj.17840.

6. Kuter E, Ahsan U, Tosun B, Karagöz DM, Gümüş H, Raza I, et al. Biomass yield, quality, nutrient composition, and feeding value of oat (*Avena sativa*) silage subjected to different wilting durations and/or inoculant application. Trop Anim Health Prod. 2023;55:299. https://doi.org/10.1007/s11250-023-03751-9.

7. Duan H, Wu R, Wang W, Zhang R, Hu Z, Liang G, et al. Stay-green trait improves yield, quality, and feeding value of forage oats under contrasting eco-sowing systems. Front Plant Sci. 2026;16:1709486. https://doi.org/10.3389/fpls.2025.1709486.

8. Chen H, Xue L, White JF, Kamran M, Li C. Identification and characterization of Pyrenophora species causing leaf spot on oat (*Avena sativa*) in western China. Plant Pathol. 2022;71:566–77. https://doi.org/10.1111/ppa.13491.

9. Wang Z, Niu K, Zhao G, Zhang Y, Chai J, Ju Z. Exogenous 24-epibrassinolide improves resistance to leaf spot disease through antioxidant regulation and phenylpropanoid metabolism in oats. Agronomy. 2024;14:3035. https://doi.org/10.3390/agronomy14123035.

10. Torres Ascurra YC, Schrammel B, Monino-Lopez D, Merino Martin G, Wiedmer J, Vleeshouwers VGAA. Diversification and deployment of PRR and NLR immune receptors in potato. Plant J. 2026;127:e71002. https://doi.org/10.1111/tpj.71002.

11. Jones JDG, Staskawicz BJ, Dangl JL. The plant immune system: From discovery to

deployment. Cell. 2024;187:2095–116. https://doi.org/10.1016/j.cell.2024.03.045.

12. Yu XQ, Niu HQ, Liu C, Wang HL, Yin W, Xia X. PTI–ETI synergistic signal mechanisms in plant immunity. Plant Biotechnol J. 2024;22:2113–28. https://doi.org/10.1111/pbi.14332.

13. Liu J, Li W, Wu G, Ali K. An update on evolutionary, structural, and functional studies of receptor-like kinases in plants. Front Plant Sci. 2024;15:1305599. https://doi.org/10.3389/fpls.2024.1305599.

14. Liu Q, Fu Q, Yan Y, Jiang Q, Mao L, Wang L, et al. Curation, nomenclature, and topological classification of receptor-like kinases from 528 plant species for novel domain discovery and functional inference. Mol Plant. 2024;17:658–71. https://doi.org/10.1016/j.molp.2024.02.015.

15. Cai M, Yu H, Sun E, Zuo C. Receptor-like proteins: Decision-makers of plant immunity. Phytopathol Res. 2024;6:58. https://doi.org/10.1186/s42483-024-00279-0.

16. Hailemariam S, Liao CJ, Mengiste T. Receptor-like cytoplasmic kinases: Orchestrating plant cellular communication. Trends Plant Sci. 2024;29:1113–30. https://doi.org/10.1016/j.tplants.2024.04.006.

17. Wang J, Bai L, Xu Y, Zheng X, Shan W, Shi X, et al. Receptor-like cytoplasmic kinases mediated signaling in plant immunity: Convergence and divergence. Stress Biol. 2025;5:43. https://doi.org/10.1007/s44154-025-00219-8.

18. Qiao X, Li Q, Yin H, Qi K, Li L, Wang R, et al. Gene duplication and evolution in recurring polyploidization–diploidization cycles in plants. Genome Biol.

651 2019;20:38. https://doi.org/10.1186/s13059-019-1650-2.
652 19. Chen H, Zhang Y, Feng S. Whole-genome and dispersed duplication, including
653 transposed duplication, jointly advance the evolution of TLP genes in seven
654 representative Poaceae lineages. BMC Genomics. 2023;24:290.
655 https://doi.org/10.1186/s12864-023-09389-z.
656 20. Zhang T, Huang W, Zhang L, Li DZ, Qi J, Ma H. Phylogenomic profiles of whole-
657 genome duplications in Poaceae and landscape of differential duplicate retention
658 and losses among major Poaceae lineages. Nat Commun. 2024;15:3305.
659 https://doi.org/10.1038/s41467-024-47428-9.
660 21. Cisneros AF, Dibyachintan S, Bédard F, Aubé S, Lemieux P, Landry CR.
661 Evolutionary causes and consequences of gene duplication. Nat Rev Genet.
662 2026;27:512–29. https://doi.org/10.1038/s41576-026-00935-5.
663 22. Li LL, Xiao Y, Wang X, He ZH, Lv YW, Hu XS. The Ka/Ks and πa/πs ratios under
664 different models of gametophytic and sporophytic selection. Genome Biol Evol.
665 2023;15:evad151. https://doi.org/10.1093/gbe/evad151.
666 23. Del Amparo R, Branco C, Arenas J, Vicens A, Arenas M. Analysis of selection in
667 protein-coding sequences accounting for common biases. Brief Bioinform.
668 2021;22:bbaa431. https://doi.org/10.1093/bib/bbaa431.
669 24. Zhang N, Tang L, Li S, Liu L, Gao M, Wang S, et al. Integration of multi-omics
670 data accelerates molecular analysis of common wheat traits. Nat Commun.
671 2025;16:2200. https://doi.org/10.1038/s41467-025-57550-x.
672 25. Avni R, Kamal N, Bitz L, Jellen EN, Bekele WA, Angessa TT, et al. A pangenome

673 and pantranscriptome of hexaploid oat. Nature. 2026;649:131–9.
674 https://doi.org/10.1038/s41586-025-09676-7.
675 26. Peng Y, Yan H, Guo L, Deng C, Wang C, Wang Y, et al. Reference genome
676 assemblies reveal the origin and evolution of allohexaploid oat. Nat Genet.
677 2022;54:1248–58. https://doi.org/10.1038/s41588-022-01127-7.
678 27. He Q, Li W, Miao Y, Wang Y, Liu N, Liu J, et al. The near-complete genome
679 assembly of hexaploid wild oat reveals its genome evolution and divergence with
680 cultivated oats. Nat Plants. 2024;10:2062–78. https://doi.org/10.1038/s41477-
681 024-01866-x.
682 28. Chinchilla D, Zipfel C, Robatzek S, Kemmerling B, Nürnberger T, Jones JDG, et
683 al. A flagellin-induced complex of the receptor FLS2 and BAK1 initiates plant
684 defence. Nature. 2007;448:497–500. https://doi.org/10.1038/nature05999.
685 29. Wang C, Wang G, Zhang C, Zhu P, Dai H, Yu N, et al. OsCERK1-mediated chitin
686 perception and immune signaling requires receptor-like cytoplasmic kinase 185 to
687 activate an MAPK cascade in rice. Mol Plant. 2017;10:619–33.
688 https://doi.org/10.1016/j.molp.2017.01.006.
689 30. Liu X, Yang C, Dong H, Wu S, Wang G, Han X, et al. TaRLK2.4, a transgressive
690 expression receptor like kinase, improves powdery mildew resistance in wheat. Int
691 J Biol Macromol. 2024;277 Pt 4:134387.
692 https://doi.org/10.1016/j.ijbiomac.2024.134387.
693 31. He M, Zhang S, Tang C, Yan Y, Zhang Z, Wang J, et al. TaWAKL8-2B, a wall-
694 associated receptor-like kinase, mediates wheat rust resistance by linalool and

695 ROS accumulation. Stress Biol. 2025;5:50. https://doi.org/10.1007/s44154-025-
696 00248-3.
697 32. Yin Z, Liu J, Dou D. RLKdb: A comprehensively curated database of plant receptor-
698 like kinase families. Mol Plant. 2024;17:513–5.
699 https://doi.org/10.1016/j.molp.2024.02.014.
700 33. Xiong G, Cui D, Tian Y, Schwarzacher T, Heslop-Harrison JS, Liu Q. Genome-wide
701 identification of the lectin receptor-like kinase gene family in *Avena sativa* and its
702 role in salt stress tolerance. Int J Mol Sci. 2024;25:12754.
703 https://doi.org/10.3390/ijms252312754.
704 34. Ma A, Liu T, Tian W, Chen H, Wang G, Zhang B. Physiological and molecular
705 profiling unveils oat (*Avena sativa* L.) defense mechanisms against powdery
706 mildew. Front Plant Sci. 2025;16:1580472.
707 https://doi.org/10.3389/fpls.2025.1580472.
708 35. Eddy SR. Accelerated Profile HMM Searches. PLoS Comput Biol.
709 2011;7:e1002195. https://doi.org/10.1371/journal.pcbi.1002195.
710 36. Lehti-Shiu MD, Shiu SH. Diversity, classification and function of the plant protein
711 kinase superfamily. Philos Trans R Soc Lond B Biol Sci. 2012;367:2619–39.
712 https://doi.org/10.1098/rstb.2012.0003.
713 37. Sun J, Li L, Wang P, Zhang S, Wu J. Genome-wide characterization, evolution, and
714 expression analysis of the leucine-rich repeat receptor-like protein kinase gene
715 family in Rosaceae genomes. BMC Genomics. 2017;18:763.
716 https://doi.org/10.1186/s12864-017-4155-y.

717 38. Fu L, Niu B, Zhu Z, Wu S, Li W. CD-HIT: accelerated for clustering the next-
718 generation sequencing data. Bioinformatics. 2012;28:3150–2.
719 https://doi.org/10.1093/bioinformatics/bts565.
720 39. Paysan-Lafosse T, Andreeva A, Blum M, Chuguransky SR, Grego T, Pinto BL, et
721 al. The Pfam protein families database: embracing AI/ML. Nucleic Acids Res.
722 2025;53 D1:D523–34. https://doi.org/10.1093/nar/gkae997.
723 40. Blum M, Andreeva A, Florentino LC, Chuguransky SR, Grego T, Hobbs E, et al.
724 InterPro: the protein sequence classification resource in 2025. Nucleic Acids Res.
725 2025;53 D1:D444–56. https://doi.org/10.1093/nar/gkae1082.
726 41. Jones P, Binns D, Chang HY, Fraser M, Li W, McAnulla C, et al. InterProScan 5:
727 genome-scale protein function classification. Bioinformatics. 2014;30:1236–40.
728 https://doi.org/10.1093/bioinformatics/btu031.
729 42. Katoh K, Standley DM. MAFFT Multiple Sequence Alignment Software Version 7:
730 Improvements in Performance and Usability. Mol Biol Evol. 2013;30:772–80.
731 https://doi.org/10.1093/molbev/mst010.
732 43. Capella-Gutiérrez S, Silla-Martínez JM, Gabaldón T. trimAl: a tool for automated
733 alignment trimming in large-scale phylogenetic analyses. Bioinformatics.
734 2009;25:1972–3. https://doi.org/10.1093/bioinformatics/btp348.
735 44. Price MN, Dehal PS, Arkin AP. FastTree 2—approximately maximum-likelihood
736 trees for large alignments. PLoS ONE. 2010;5:e9490.
737 https://doi.org/10.1371/journal.pone.0009490.
738 45. Letunic I, Bork P. Interactive Tree of Life (iTOL) v6: recent updates to the

phylogenetic tree display and annotation tool. Nucleic Acids Res. 2024;52 W1:W78–82. https://doi.org/10.1093/nar/gkae268.

46. Minh BQ, Schmidt HA, Chernomor O, Schrempf D, Woodhams MD, von Haeseler A, et al. IQ-TREE 2: New Models and Efficient Methods for Phylogenetic Inference in the Genomic Era. Mol Biol Evol. 2020;37:1530–4. https://doi.org/10.1093/molbev/msaa015.

47. Vernot B, Stolzer M, Goldman A, Durand D. Reconciliation with non-binary species trees. J Comput Biol. 2008;15:981–1006. https://doi.org/10.1089/cmb.2008.0092.

48. Emms DM, Kelly S. OrthoFinder: phylogenetic orthology inference for comparative genomics. Genome Biol. 2019;20:238. https://doi.org/10.1186/s13059-019-1832-y.

49. Buchfink B, Reuter K, Drost HG. Sensitive protein alignments at tree-of-life scale using DIAMOND. Nat Methods. 2021;18:366–8. https://doi.org/10.1038/s41592-021-01101-x.

50. Suyama M, Torrents D, Bork P. PAL2NAL: robust conversion of protein sequence alignments into the corresponding codon alignments. Nucleic Acids Res. 2006;34 Web Server issue:W609–12. https://doi.org/10.1093/nar/gkl315.

51. Wang D, Zhang Y, Zhang Z, Zhu J, Yu J. KaKs_Calculator 2.0: A Toolkit Incorporating Gamma-Series Methods and Sliding Window Strategies. Genomics Proteomics Bioinformatics. 2010;8:77–80. https://doi.org/10.1016/S1672-0229(10)60008-3.

52. Cao Y, Chai J, Niu K, Zeng L, Wang W, Huang P, et al. Transcriptomic and

761 metabolomic analyses reveal early coordination between redox homeostasis and
762 phenylpropanoid metabolism associated with oat resistance to *Drechslera avenae*.
763 BMC Plant Biol. 2026. https://doi.org/10.1186/s12870-026-09709-x.
764 53. Langfelder P, Horvath S. WGCNA: an R package for weighted correlation network
765 analysis. BMC Bioinformatics. 2008;9:559. https://doi.org/10.1186/1471-2105-9-
766 559.
767 54. Langfelder P, Zhang B, Horvath S. Defining clusters from a hierarchical cluster tree:
768 the Dynamic Tree Cut package for R. Bioinformatics. 2008;24:719–20.
769 https://doi.org/10.1093/bioinformatics/btm563.
770 55. Xu S, Hu E, Cai Y, Xie Z, Luo X, Zhan L, et al. Using clusterProfiler to characterize
771 multiomics data. Nat Protoc. 2024;19:3292–320. https://doi.org/10.1038/s41596-
772 024-01020-z.
773 56. Kanehisa M, Furumichi M, Sato Y, Matsuura Y, Ishiguro-Watanabe M. KEGG:
774 biological systems database as a model of the real world. Nucleic Acids Res.
775 2025;53 D1:D672–7. https://doi.org/10.1093/nar/gkae909.
776 57. Lescot M, Déhais P, Thijs G, Marchal K, Moreau Y, Van de Peer Y, et al. PlantCARE,
777 a database of plant cis-acting regulatory elements and a portal to tools for in silico
778 analysis of promoter sequences. Nucleic Acids Res. 2002;30:325–7.
779 https://doi.org/10.1093/nar/30.1.325.
780 58. Gasteiger E, Hoogland C, Gattiker A, Duvaud S, Wilkins MR, Appel RD, et al.
781 Protein Identification and Analysis Tools on the ExPASy Server. In: Walker JM,
782 editor. The Proteomics Protocols Handbook. Totowa, NJ: Humana Press; 2005. p.

783 571–607. https://doi.org/10.1385/1-59259-890-0:571.
784 59. Teufel F, Almagro Armenteros JJ, Johansen AR, Gíslason MH, Pihl SI, Tsirigos KD,
785 et al. SignalP 6.0 predicts all five types of signal peptides using protein language
786 models. Nat Biotechnol. 2022;40:1023–5. https://doi.org/10.1038/s41587-021-
787 01156-3.
788 60. Cheng F, Wu J, Cai X, Liang J, Freeling M, Wang X. Gene retention, fractionation
789 and subgenome differences in polyploid plants. Nat Plants. 2018;4:258–68.
790 https://doi.org/10.1038/s41477-018-0136-7.
791 61. Li Z, McKibben MTW, Finch GS, Blischak PD, Sutherland BL, Barker MS.
792 Patterns and processes of diploidization in land plants. Annu Rev Plant Biol.
793 2021;72:387–410. https://doi.org/10.1146/annurev-arplant-050718-100344.
794 62. Paterson AH, Queitsch C. Genome organization and botanical diversity. Plant Cell.
795 2024;36:1186–204. https://doi.org/10.1093/plcell/koae045.
796 63. Yan J, Su P, Meng X, Liu P. Phylogeny of the plant receptor-like kinase (RLK) gene
797 family and expression analysis of wheat RLK genes in response to biotic and
798 abiotic stresses. BMC Genomics. 2023;24:224. https://doi.org/10.1186/s12864-
799 023-09303-7.
800 64. Gawande ND, Sankaranarayanan S. Genome wide characterization and expression
801 analysis of CrRLK1L gene family in wheat unravels their roles in development
802 and stress-specific responses. Front Plant Sci. 2024;15:1345774.
803 https://doi.org/10.3389/fpls.2024.1345774.
804 65. Ezoe A, Todaka D, Utsumi Y, Takahashi S, Kawaura K, Seki M. Decrease in

805 purifying selection pressures on wheat homoeologous genes: tetraploidization
806 versus hexaploidization. Plant J. 2024;120:1190–205.
807 https://doi.org/10.1111/tpj.17047.
808 66. Saintenac C, Cambon F, Aouini L, Verstappen E, Ghaffary SMT, Poucet T, et al. A
809 wheat cysteine-rich receptor-like kinase confers broad-spectrum resistance against
810 Septoria tritici blotch. Nat Commun. 2021;12:433.
811 https://doi.org/10.1038/s41467-020-20685-0.
812 67. Hafeez AN, Chartrain L, Feng C, Cambon F, Clarke M, Griffiths S, et al. Septoria
813 tritici blotch resistance gene Stb15 encodes a lectin receptor-like kinase. Nat Plants.
814 2025;11:410–20. https://doi.org/10.1038/s41477-025-01920-2.
815 68. Niu E, Zhang Y, Xu H, Xu B, Liang Q, Li H, et al. A G-type lectin receptor-like
816 kinase TaSRLK confers wheat resistance to stripe rust by regulating the reactive
817 oxygen species signaling pathway. Stress Biol. 2025;5:37.
818 https://doi.org/10.1007/s44154-025-00225-w.
819 69. Guo F, Wu T, Shen F, Xu G, Qi H, Zhang Z. The cysteine-rich receptor-like kinase
820 TaCRK3 contributes to defense against *Rhizoctonia cerealis* in wheat. J Exp Bot.
821 2021;72:6904–19. https://doi.org/10.1093/jxb/erab328.
822 70. Qi H, Guo F, Lv L, Zhu X, Zhang L, Yu J, et al. The wheat wall-associated receptor-
823 like kinase TaWAK-6D mediates broad resistance to two fungal pathogens
824 *Fusarium pseudograminearum* and *Rhizoctonia cerealis*. Front Plant Sci.
825 2021;12:758196. https://doi.org/10.3389/fpls.2021.758196.
826 71. Hurni S, Scheuermann D, Krattinger SG, Kessel B, Wicker T, Herren G, et al. The

827 maize disease resistance gene Htn1 against northern corn leaf blight encodes a
828 wall-associated receptor-like kinase. Proc Natl Acad Sci U S A. 2015;112:8780–5.
829 https://doi.org/10.1073/pnas.1502522112.
830 72. Duan Y, Wang Z, Fang Y, Pei Z, Hu H, Xu Q, et al. A secreted fungal laccase targets
831 the receptor kinase OsSRF3 to inhibit OsBAK1–OsSRF3-mediated immunity in
832 rice. Nat Commun. 2024;15:7891. https://doi.org/10.1038/s41467-024-52204-w.
833 73. Kang WH, Lee J, Koo N, Kwon JS, Park B, Kim YM, et al. Universal gene co-
834 expression network reveals receptor-like protein genes involved in broad-
835 spectrum resistance in pepper (*Capsicum annuum* L.). Hortic Res. 2022;9:uhab003.
836 https://doi.org/10.1093/hr/uhab003.
837 74. Wang R, Wang Y, Yao W, Ge W, Jiang T, Zhou B. Transcriptome sequencing and
838 WGCNA reveal key genes in response to leaf blight in poplar. Int J Mol Sci.
839 2023;24:10047. https://doi.org/10.3390/ijms241210047.
840 75. Zhao G, Qin S, Wei Z, Bai X, Guo J, Kang Z, et al. Evolutionary characteristics,
841 expression patterns of wheat receptor-like kinases and functional analysis of
842 TaCrRLK1L16. Stress Biol. 2025;5:24. https://doi.org/10.1007/s44154-025-
843 00215-y.
844 76. Koley P, Brahmachari S, Saha A, Deb C, Mondal M, Das N, et al. Phytohormone
845 priming of tomato plants evoke differential behavior in *Rhizoctonia solani* during
846 infection, with salicylate priming imparting greater tolerance than jasmonate.
847 Front Plant Sci. 2022;12:766095. https://doi.org/10.3389/fpls.2021.766095.
848 77. Dinolfo MI, Martínez M, Castañares E, Vanzetti LS, Rossi F, Stenglein SA, et al.

Interaction of methyl-jasmonate and *Fusarium poae* in bread wheat. Fungal Biol. 2022;126:786–92. https://doi.org/10.1016/j.funbio.2022.10.002.

78. Gao J, Sun Y, Jin W, Zhang F, Zhou M, Song X. Methyl jasmonate mitigates *Fusarium graminearum* infection in wheat by inhibiting deoxynivalenol synthesis. Physiol Plant. 2024;176:e14593. https://doi.org/10.1111/ppl.14593.

Supplementary Files

This is a list of supplementary files associated with this preprint. Click to download.

- Additionaltables.xlsx
- Additionalfile.docx